THE ASTROPHYSICAL JOURNAL, 567:L89–L92, 2002 March 1
© 2002. The American Astronomical Society. All rights reserved. Printed in U.S.A.

STEADY FLOWS DETECTED IN EXTREME-ULTRAVIOLET LOOPS

AMY R. WINEBARGER,[1] HARRY WARREN, ADRIAAN VAN BALLEGOOIJEN, EDWARD E. DELUCA, AND LEON GOLUB
Harvard-Smithsonian Center for Astrophysics, 60 Garden Street, Cambridge, MA 02138; awinebarger@cfa.harvard.edu, hwarren@cfa.harvard.edu, avanballegooijen@cfa.harvard.edu, edeluca@cfa.harvard.edu, lgolub@cfa.harvard.edu
Received 2001 November 14; accepted 2002 January 23; published 2002 February 12

ABSTRACT

Recent *Transition Region and Coronal Explorer* (*TRACE*) observations have detected a class of active region loops whose physical properties are inconsistent with previous hydrostatic loop models. In this Letter we present the first co-aligned *TRACE* and the Solar Ultraviolet Measurement of Emitted Radiation (SUMER) observations of these loops. Although these loops appear static in the *TRACE* images, SUMER detects line-of-sight flows along the loops of up to 40 km s^{-1}. The presence of flows could imply an asymmetric heating function; such a heating function would be expected for heating that is proportional to (often asymmetric) footpoint field strength. We compare a steady flow solution resulting from an asymmetric heating function to a static solution resulting from a uniform heating function in a hypothetical coronal loop. We find that the characteristics associated with the asymmetrically heated loop better compare with the characteristics of the loops observed in the *TRACE* data.

Subject heading: Sun: corona

1. INTRODUCTION

The determination of the heating mechanism in the solar corona is a fundamental problem in solar physics. To address this problem, Rosner, Tucker, & Vaiana (1978) derived scaling laws that describe the relationship between the energy deposited in a coronal loop and the resulting temperature and density along the loop. In their model, they simplified the energy balance equation by assuming constant pressure, uniform heating, and a static semicircular loop with constant cross section. This model was later appended to include the effects of gravity and a possible heating scale height (Serio et al. 1981). (The standard hydrostatic model including gravity is referred to as the Rosner-Tucker-Vaiana-Serio model, hereafter the RTVS model.) Emission from high-temperature loops observed with X-ray instruments was found to support the RTVS model (e.g., Kano & Tsuneta 1996).

The RTVS model predicts a steep temperature rise from the loop footpoint through the transition region and a small but measurable temperature increase from the top of the transition region to the loop apex. It further predicts an exponential decrease in pressure due to gravity. Several recent EUV studies have discovered a class of active region loops that do not agree with the temperature and pressure stratification predicted by the RTVS model (Gabriel 1976; Aschwanden, Nightengale, & Alexander 2000; Lenz et al. 1999a, 1999b). The loops exhibit a flat 195 Å/171 Å filter ratio along their lengths; the RTVS model would predict gradients in the filter ratios. The intensity along the loops also does not decrease as would be predicted by the pressure exponentially decreasing with a gravitational scale height.

The previous attempts to explain the flat filter ratios and enhanced intensity have fallen into two categories: (1) the observed loop is interpreted as a bundle of small filaments, each individually obeying hydrostatic scaling laws (Reale & Peres 2000; Aschwanden et al. 2000), and (2) the loop is treated as a single structure and is described by a single set of hydrostatic equations (Litwin & Rosner 1998; Aschwanden, Schrijver, & Alexander 2001). In both cases, the modelers have assumed that the heating within the structure(s) is symmetric and have not considered the possibility of flows along the loops.

In this Letter we present joint *Transition Region and Coronal Explorer* (*TRACE*) and Solar Ultraviolet Measurement of Emitted Radiation (SUMER) observations of NOAA Active Region 8536 on 1999 May 13 at 13:00–15:00 UT. The active region contains several examples of typical EUV loops; a portion of these loops was scanned by SUMER. Although these loops appear static over the *TRACE* observations, we find line-of-sight velocities in these loops of 15–40 (± 5) km s^{-1} from shifts in the Ne VIII spectral line. These velocities provide an important diagnostic (similar to the filter ratio and intensity) in constraining the coronal heating mechanism. They suggest a need for a steady flow or dynamic treatment of the hydrodynamic equations instead of the static, symmetric treatment used in previous loop models. In § 3 we compare the steady flow solution resulting from an asymmetric heating function (i.e., one footpoint is more strongly heated than the other footpoint) with the static solution that results from a uniform heating function for a representative coronal loop. We find that asymmetric heating induces flows and improves the comparison with *TRACE* and SUMER data, but it does not entirely solve the discrepancy between theory and observations.

2. DATA AND ANALYSIS

TRACE (Handy et al. 1999; Schrijver et al. 1999; Golub et al. 1999) and SUMER (Wilhelm et al. 1995, 1997; Lemaire et al. 1997) jointly observed NOAA AR 8536 from approximately 13:00 to 15:00 UT on 1999 May 13. A full-disk EUV Imaging Telescope (EIT) 171 Å image observed at 13:00 UT on 1999 May 13 is shown in the left panel of Figure 1; the *TRACE* field of view is highlighted with a box. The *TRACE* observing sequence included the 171, 195, and 1600 Å filter images taken at a cadence of ~50 s. An example of a *TRACE* 171 Å image is shown in the right panel of Figure 1.

The SUMER scan region is the box shown in the right panel of Figure 1. The SUMER observing sequence includes rastering the $1'' \times 120''$ slit with $1''.5$ steps across the SUMER scan region. A single raster over $160''$ took approximately 55 minutes; the region was scanned twice (from east to west, then from west to east) within the observing time. Five spectral windows (~2 Å

[1] Current address: US Naval Research Laboratory, Code 7673W, Washington, DC 20375; amy@dogwood.nrl.navy.mil.

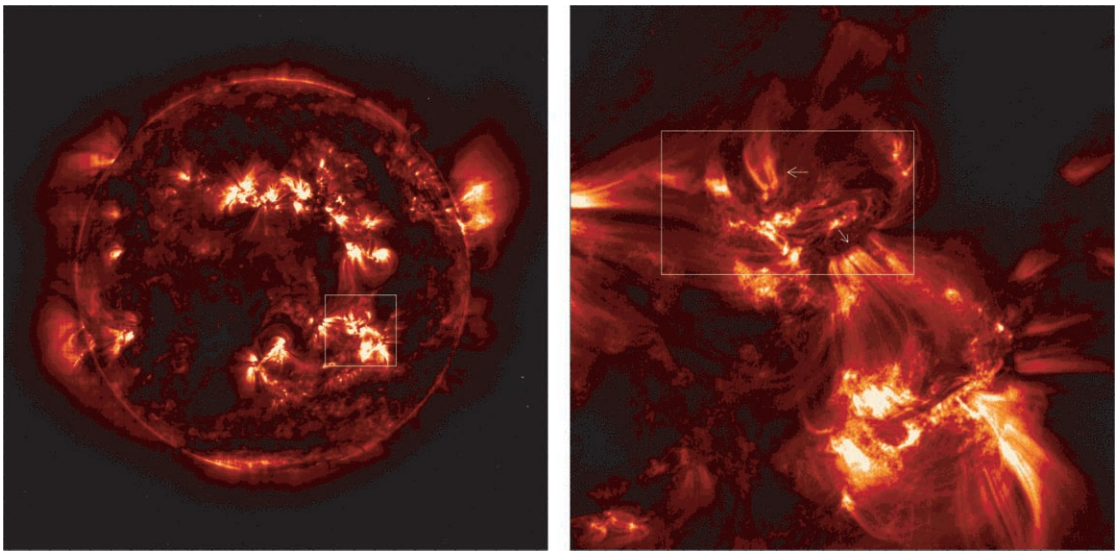

FIG. 1.—*Left panel:* EIT 171 Å image observed at 13:00 UT on 1999 May 13. *TRACE* field of view is highlighted with a box. *Right panel: TRACE* 171 Å image observed at 13:00 UT on 1999 May 13. *TRACE* field of view is 350″ × 350″. SUMER scan region is highlighted with a box; SUMER field of view is 162″ × 92″. Arrows point to the two candidate loop structures.

wide) were simultaneously observed during the main observing sequence. The analysis in this Letter focuses on the Ne VIII 770 Å line observed in second order. Before and after the main observing sequence, several full-detector (~45 Å wide) observations were recorded. These observations include several chromospheric lines (Si II λ1526.708, Si II λ1533.432, C I λ1542.177, Si I λ1545.575, Fe II λ1550.260), which we use to determine the wavelength calibration of each full-detector spectrum. The error in the resulting wavelength calibration is ≈3 km s^{-1}. Owing to temperature fluctuations in the instrument, the wavelength calibration fluctuates ≈3 km s^{-1} over time frames of 1.5 hr (e.g., Peter 1999). Hence, we believe the velocities in the spectral lines can be measured to within 5 km s^{-1}.

Two sets of fan structures are highlighted by arrows in the right panel of Figure 1. Assuming the loops are semicircular, we estimate the lengths of the loops in the upper left fan structure to be 65 Mm and those in the lower right fan structure to be 110 Mm. These loops have a constant 195 Å/171 Å filter ratio along their lengths. The intensity in these fan structures is also "steady" (intensity fluctuations are <1 DN s^{-1}) over nearly 2 hr of observations. This time frame is long compared to the sound crossing time (~20 minutes) and steady state decay time (~60 minutes; Serio et al. 1991). Hence, they have characteristics similar to loops studied in previous analyses (e.g., Lenz et al. 1999a). A portion of these loops were scanned by SUMER.

A *TRACE* 171 Å image and a spectroheliogram from the initial Ne VIII scan are shown in Figures 2*a* and 2*b*, respectively. The contours on the Ne VIII image are from the *TRACE* image. The arrows point to the two fan structures of interest. The fan structures are observable in both images, even though the emissivity function of Ne VIII peaks around $10^{5.8}$ K, while the *TRACE* 171 Å filter temperature sensitivity peaks at 10^6 K. To confirm that we were indeed imaging the same plasma in these structures, we have also compared these images with Coronal Diagnostic Spectrometer rasters taken in the same region around 13:00 UT to constrain the temperature of these loops. The structures are clearly evident in the Ca X λ558 ($10^{5.8}$ K) and Mg IX λ368 ($10^{6.0}$ K) rasters, while they are completely absent in the hotter rasters, such as Si XII λ521 ($10^{6.3}$ K). Using the average Ca X λ558, Mg IX λ368, and Ne VIII λ770 intensity in the fan structures and the emission measure loci technique (e.g., Schmelz et al. 1996), we find the average temperature in the fan structures to be $10^{5.95 \pm 0.05}$ K. This temperature corresponds to an emission measure of 1×10^{27} cm^{-5}. These values predict the intensity in the *TRACE* 171 Å filter to within a factor of 2; we therefore believe the same plasma is indeed imaged in both the *TRACE* 171 Å image and the Ne VIII spectra.

The Ne VIII line profiles were fit with Gaussian functions. The velocities were measured from the shifts in the centroids of the Gaussians from the rest wavelength of Ne VIII (770.409 Å). The resultant velocity maps of the region for the two scans are shown in Figures 2*c* and 2*d*. The contours in Figure 2 are of the *TRACE* 171 Å image at the beginning of the observing sequence; arrows point to the candidate fan structures. The Ne VIII velocities are significant: ~15–40 km s^{-1} line-of-sight flows along the candidate loops structures. These flows appear constant along the loops.

Two scans were made of this area; hence, we can also address the steadiness of the flows along these loops. However, because the scans were made in opposite directions (the first was from east to west and the second from west to east), the difference in time between the two observations of the same area varies across the image. The two scans of the fan structure on the bottom right occurred approximately 30 minutes apart. The differences in the velocities measured during these two scans are less than the error in the velocity (5 km s^{-1}). The time between the scans of the upper left structure was approximately 70 minutes. The velocities along this structure in the two scans are comparable. However, the structures themselves appear to have suffered transverse motion over the 70 minutes; hence, the structure lies outside the original contour in the velocity map from the second scan (Fig. 2*d*).

3. DISCUSSION

Through analyzing co-aligned *TRACE* and SUMER data, we find that significant line-of-sight flows can exist along the EUV loop structures even if the *TRACE* intensity appears static. This observation puts important constraints on the models of these

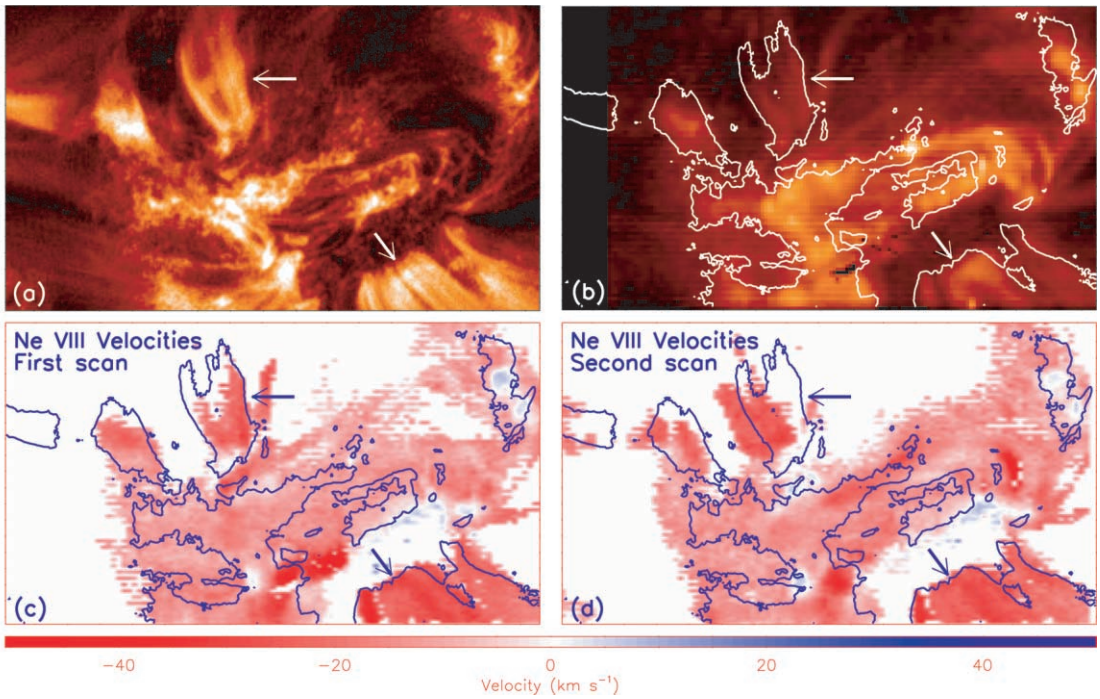

FIG. 2.—(*a*) *TRACE* 171 Å image of NOAA AR 8536 on 1999 May 13. Arrows point to fan structures that appear static throughout the 2 hr of *TRACE* observations. (*b*) Spectroheliogram of the Ne VIII λ770 line from the initial scan. Contours are from the 171 Å image. Velocities found from shifts in the Ne VIII spectral lines from the initial scan are shown in (*c*) and from the final scan are shown in (*d*).

loops. Previous models have assumed static, symmetric solutions to the hydrodynamic equations; these results imply that steady flow or dynamic solutions must be considered.

In this study all the line profiles in the fan structures are redshifted, indicating downflows. Redshifts are ubiquitous in observations of transition region emission lines; however, the velocities are typically much smaller. For example, Chae, Yun, & Poland (1998) measured downflows of 5 km s^{-1} in Ne VIII in the quiet Sun. Furthermore, most transition region emission is associated with the chromospheric network, while the emission presented in this Letter is clearly associated with coronal loop structures. Therefore, we believe that these redshifts are fundamentally different than those presented in previous analyses.

Flows can exist along loops for a variety of reasons. We believe a likely driver of flows along these loops is an asymmetric heating function. Potential field extrapolations of photospheric fields show that field strengths are often different at the different footpoints; hence, an asymmetric heating function would be consistent with the heating being dependent on footpoint field strength. To demonstrate the effects of an asymmetric heating function on a coronal loop, we have generated two solutions to the hydrodynamic equations for a theoretical 150 Mm loop using an iterative code (G. A. J. Hussain & A. van Ballegooijen 2002, in preparation). We assume the loop is semicircular and perpendicular to the solar surface, and we include gravity. In the first solution, we assume that the heating is uniform along the loop, $E_H(s) = E_{H0}$, and we choose E_{H0} so that the maximum temperature of the loop is approximately 1 MK at the loop apex. For the second solution, we allow the heating function to exponentially decrease from the footpoints and to be asymmetric, i.e.,

$$E_H(s) = \begin{cases} A_1 \exp(-s/s_{H1}), & 0 \le s \le L, \\ A_2 \exp[-(2L-s)/s_{H2}], & L \le s \le 2L, \end{cases} \quad (1)$$

where we arbitrarily choose $A_1 = 10A_2$, $s_{H1} = 15$ Mm, and s_{H2} to make both heating functions equal at $s = L$. Again, we varied the value of A_1 so that the maximum temperature in the loop was approximately 1 MK. Figure 3*a* shows the uniform (*solid line*) and the asymmetric, nonuniform (*dashed line*) heating rates along the theoretical loop. Figure 3 also shows the resulting temperature (Fig. 3*b*), density (Fig. 3*c*), and velocity (Fig. 3*d*) from the uniform heating solution (*solid lines*) and asymmetric, nonuniform heating solution (*dashed lines*). Finally, we folded the density and temperature through the *TRACE* 171 and 195 Å filter response functions; the expected 171 Å intensity along the theoretical loop is shown in Figure 3*e*, and the expected ratio of the two filters is shown in Figure 3*f*.

This example demonstrates that for asymmetric heating, the filter ratio along the loop is flatter than the filter ratio in the uniform heating solution. The asymmetric heating also results in an increase in density and hence in expected intensity along the loop in the *TRACE* 171 Å filter. Both these characteristics are observed for the EUV loops. Finally, the asymmetric heating function predicts flows along the loop of ~10 km s^{-1}. The magnitude of these flows is a function of both the magnitude of the asymmetry and the nonuniformity of the heating function.

Although an asymmetric, nonuniform heating function can approximate the observed characteristics of EUV loops, it cannot completely address all the observations. For instance, the intensity enhancements tend be 10^2–10^4 times greater than those expected from uniform heating (Aschwanden et al. 2001), while the enhancement in this theoretical loop model is a factor of only 10. Also, the magnitude of the velocities observed in NOAA AR 8536 were 3–4 times greater than the velocities in this simple example. The velocities also appeared relatively constant along the loop, while the velocities predicted by the assumed heating function are not constant along the loop. If the heating function were more nonuniform (i.e., if the scale height, s_{H1}, were smaller), we might expect to get further en-

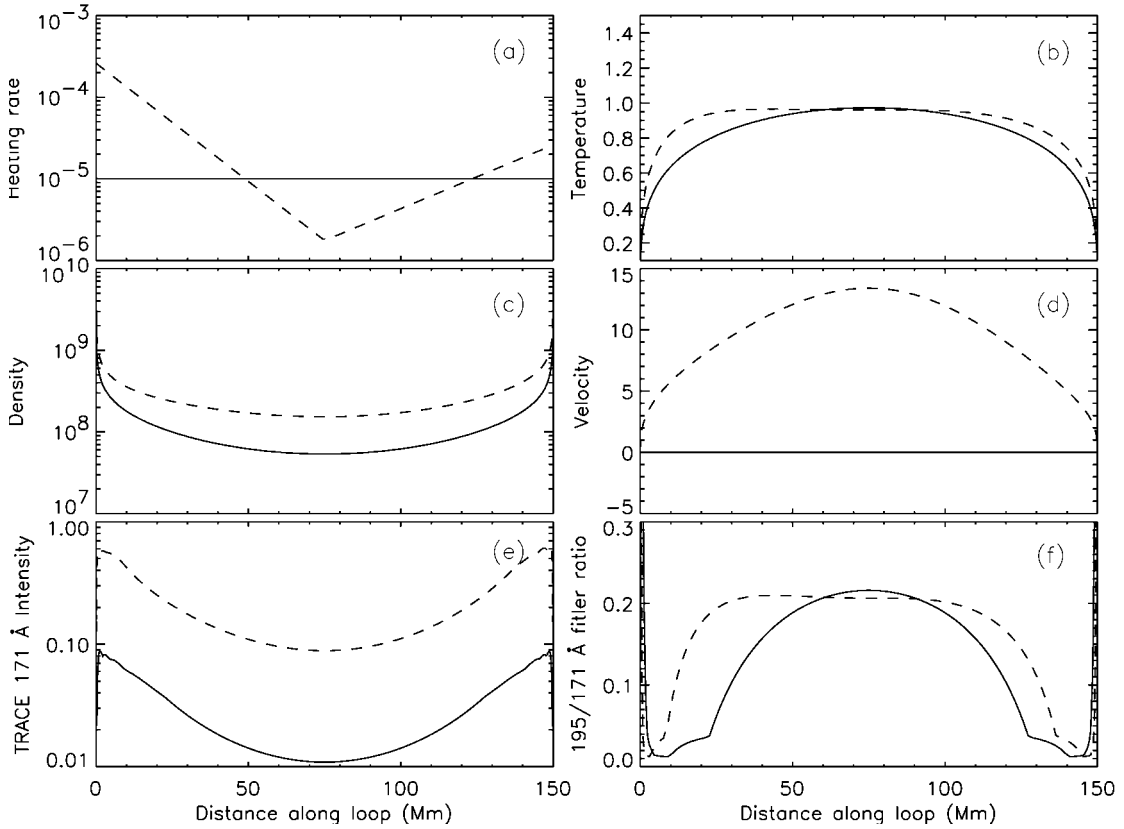

FIG. 3.—(*a*) Heating rate in units of ergs cm^{-3} s^{-1}, (*b*) temperature in MK, (*c*) density in cm^{-3}, (*d*) velocity in km s^{-1}, (*e*) expected *TRACE* 171 Å intensity in DN s^{-1}, and (*f*) expected *TRACE* 195 Å/171 Å filter ratio along a 150 Mm coronal loop for uniform heating (*solid line*) and for asymmetric, nonuniform heating (*dashed line*).

hancements in the intensity and velocity. However, there are no stable steady flow solutions for smaller scale heights (Aschwanden et al. 2001).

We have shown that the inclusion of asymmetric heating and flows in coronal loop models improves the comparison with the *TRACE* and SUMER observations, although it does not entirely solve the discrepancy between theory and observations. We speculate that other effects, such as momentum addition due to waves or dynamic processes, may also be important. Models that include wave pressure effects will be discussed in a future paper.

TRACE is supported by contract NAS 5-38099 from NASA to the Lockheed Martin Advanced Technology Center.

REFERENCES

Aschwanden, M. J., Nightingale, R. W., & Alexander, D. 2000, ApJ, 541, 1059
Aschwanden, M. J., Schrijver, C. J., & Alexander, D. 2001, ApJ, 550, 1036
Chae, J., Yun, H. S., & Poland, A. I. 1998, ApJS, 114, 151
Gabriel, A. H. 1976, Philos. Trans. R. Soc. London A, 281, 339
Golub, L., et al. 1999, Phys. Plasmas, 6, 2205
Handy, B. N., et al. 1999, Sol. Phys., 187, 229
Kano, R., & Tsuneta, S. 1996, PASJ, 48, 535
Lemaire, P., et al. 1997, Sol. Phys., 170, 105
Lenz, D. D., DeLuca, E. E., Golub, L., Rosner, R., & Bookbinder, J. A. 1999a, ApJ, 517, L155
Lenz, D. D., et al. 1999b, Sol. Phys., 190, 131
Litwin, C., & Rosner, R. 1998, ApJ, 506, L143
Peter, H. 1999, ApJ, 516, 490
Reale, F., & Peres, G. 2000, ApJ, 528, L45
Rosner, R., Tucker, W. H., & Vaiana, G. S. 1978, ApJ, 220, 643
Schmelz, J. T., Saba, J. L. R., Ghosh, D., & Strong, K. T. 1996, ApJ, 473, 519
Schrijver, C. J., et al. 1999, Sol. Phys., 187, 261
Serio, S., Peres, G., Vaiana, G. S., Golub, L., & Rosner, R. 1981, ApJ, 243, 288
Serio, S., Reale, F., Jakimiec, J., Sylwester, B., & Sylwester, J. 1991, A&A, 241, 197
Wilhelm, K., et al. 1995, Sol. Phys., 162, 189
———. 1997, Sol. Phys., 170, 75